Chapter 4

Non-Coherent UWB Communications

Nuan Song, Mike Wolf and Martin Haardt

Additional information is available at the end of the chapter

http://dx.doi.org/10.5772/53219

1. Introduction

The use of ultra wide band (UWB) signals can offer many advantages for communications. It can provide a very robust performance even under harsh multipath and interference conditions, the capability of precision ranging and a reduced power consumption. Since the power spectral density is very low, it is possible to overlay UWB networks with already existing non-UWB emissions.

Early UWB concepts for communications have almost exclusively relied on impulse radio, where the whole available bandwidth, i.e., up to 7.5 GHz, is covered at once by means of very short pulses which are generated with a low duty cycle. Meanwhile, a bandwidth of 7.5 GHz is only available in the US [1, 3]. In Europe, the spectrum which is available with the same transmit power spectral density of -41.3 dBm/MHz ranges only from 6.0 to 8.5 GHz [4], if no detect and avoid techniques are applied[1]. A potential UWB system has therefore to be able to 'live' with a mean transmit power of less than -7.3 dBm.

This is a small value, but fortunately UWB systems may exploit the signal energy very efficiently because firstly, even at data rates in the Gbps range, it is not required to use bandwidth efficient (but energy inefficient) modulation schemes like a 1024-QAM. Secondly, UWB transmission benefits from a good fading resistance.

For a measured indoor channel [7], Fig. 1 shows that even a bandwidth of 'only' 500 MHz ensures a very good fading resistance: If the receiver is moved over all x-y-positions in the non-LOS case, the smallest power value at the receive antenna lies less than 3 dB below the mean power, averaged over all positions. Thus the fading margin could be chosen in the order of 3-4 dB — even for indoor channels which exhibit the largest coherence bandwidth.

The second energy efficiency argument claimed above is underpinned in Fig. 2. It shows the channel capacity depending on the bandwidth, where additive white Gaussian noise (AWGN) is assumed. A value of 83 MHz just corresponds to the total bandwidth available in the 2.4 GHz ISM band, which is chosen for comparison. At 1 Gbps, a 2.5 GHz bandwidth promises an advantage of 25 dB with respect to the required receive-power. Furthermore, even binary modulation (on the inphase and quadrature components) promises high data rates.

[1] With detect and avoid techniques, -41.3 dBm/MHz is also permitted between 4.2 and 4.8 GHz.

Unfortunately, a very large signal bandwidth is also associated with some serious problems. These problems are related to the transceiver components itself (availability of broadband antennas, amplifiers etc.), and to the technical effort which is required for synchronization, channel estimation and interference rejection. Since UWB networks operate in frequency bands already assigned to other RF-systems, the probability that narrowband interference occurs at all increases with the bandwidth, too.

Furthermore, by increasing the bandwidth, more and more multipath arrivals with different path gains and delays are resolvable at the receiver, which makes it more difficult to collect the multipath energy coherently — although the power at the receive antenna does not suffer from the fading effect. Fig. 1 shows an example that one may lose 10 dB and more, if an UWB-receiver uses only the strongest signal echo. Thus, especially in non-LOS scenarios, a coherent RAKE receiver requires a very large number of RAKE fingers and a precise channel knowledge to efficiently capture the multipath energy. Such a coherent RAKE receiver will be very complex and costly, such that the hardware itself may consume a lot of power. This fact is the major motivation for systems using non-coherent detection, which are discussed in this chapter.

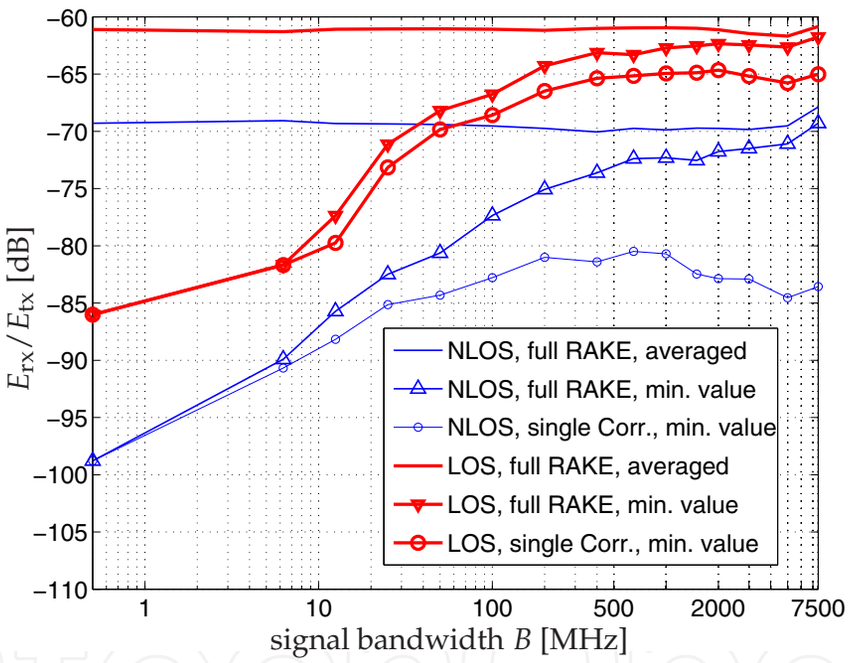

Figure 1. Received energy E_{rx} normalized by the transmitted symbol's energy E_{tx} in dB, versus different signal bandwidths. The thickness of the curves indicates LOS or non-LOS regimes. The curves without markers show E_{rx}/E_{tx} averaged across all x-y-positions within an rectangular area of 30 cm $\times$ 40 cm (1 cm grid, data from [7]), if an ideal full RAKE-receiver is used. The curves marked with triangles show the minimum value of E_{rx}/E_{tx} which occurs within these positions, again assuming a full RAKE. Thus the small-scale fading effect becomes visible. The curves with circles depict the normalized receive energy for a receiver which exploits only the strongest propagation path, i.e., a single correlator is applied. Transmitters-receiver separation is about 3 m, the carrier frequency is always set to 6.85 GHz.

Non-coherent UWB transmission is an attractive approach especially if simple and robust implementations with a small power consumption are required. Main application fields are low data rate sensor or personal area networks, which require low cost devices and a long battery life time. It should be noted that the current IEEE802.15.4a UWB-PHY for low data rate communications enables non-coherent detection, too [18]. The main advantage of a

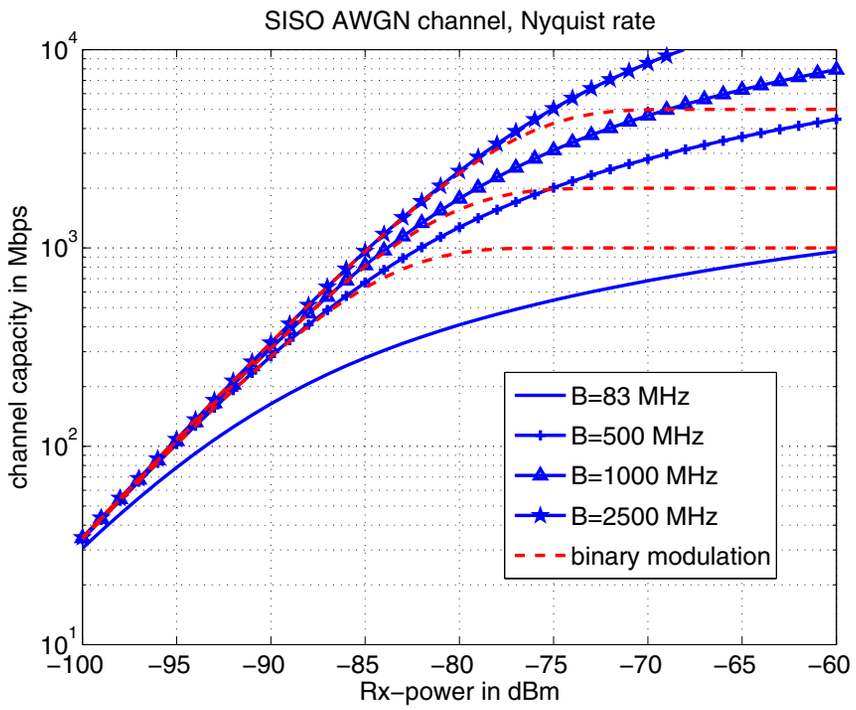

Figure 2. Capacity of an AWGN channel as a function of the receive-power for different signal bandwidths. The 2.4 GHz ISM band offers a bandwidth of 83 MHz.

non-coherent receiver is clearly the dramatically reduced effort which is required for channel estimation, synchronization, and multipath diversity combining. This advantage is, however, bought by a serious drawback: non-coherent detectors are more susceptible to narrowband interference (NBI), multi-user interference (MUI), and inter-symbol interference (ISI).

Non-coherent detection can either rely on envelope detection or on differential detection. In the simplest case, path-diversity combining is carried out via an analog integration device. However, the change from analog to digital combining stimulates new perspectives. Since a digital code matched filter can be applied prior to the non-coherent part of the receiver, the capability to distinguish users (or networks) by means of code division multiple access is improved. We show that digital receiver implementations with user specific filtering have also an enhanced interference rejection capability and energy efficiency. Moreover, we present well suited solutions for the analog-to-digital conversion, the spread-spectrum code sequences, and the modulation format.

2. Non-coherent detection in multipath AWGN

Although non-coherent detection is not restricted to low data rates — even orthogonal frequency division multiplex (OFDM) can be combined with non-coherent modulation and detection [19] — we focus our attention on low data rate single carrier transmission.

Non-coherent detection can either be based on envelope detection or on differential detection. In the simplest case, path-diversity combining can be achieved by means of a single, analog integrate and dump filter, see Fig. 3 and Fig. 4. The integration effectively provides a binary weighting of the multipath arrivals: all components inside the integration window of size T_{int} are weighted with "1", while all the others are weighted with "0". Regardless of whether envelope or differential detection is chosen, we assume that the receiver uses a quadrature

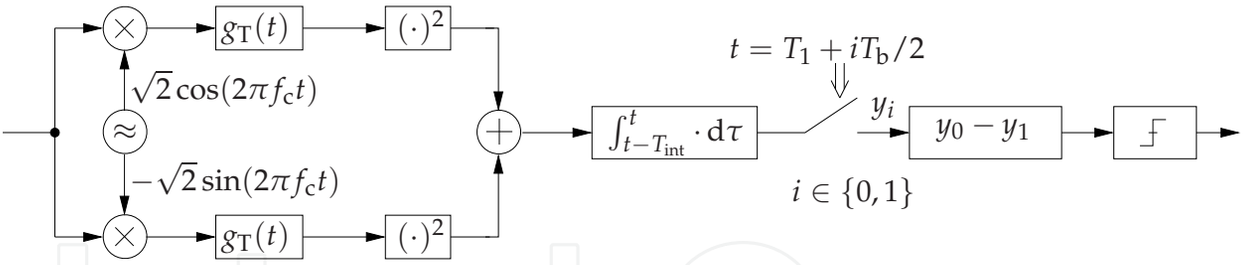

Figure 3. Envelope detection of a 2-PPM signal using a quadrature down-conversion stage. The analog integrate and dump filter (integrator) is required to capture the multipath energy.

down-conversion stage, since an ECC-conform UWB-signal is a 'truth' band-pass signal with a maximum bandwidth of 2.5 GHz and a lower cut-on frequency of 6 GHz. It is also assumed that each the inphase and the quadrature branch contain a low-pass filter, whose impulse response $g_T(t)$ is matched to the transmitted pulse $\psi_1(t)$. Without multipath, this ensures that the energy of the received signal is focused at the sampling times. For example, according to the IEEE 802.15.4a UWB PHY standard a receiver needs to perform a matched de-chirp operation, if the optional "chirp on UWB" pulse is used.

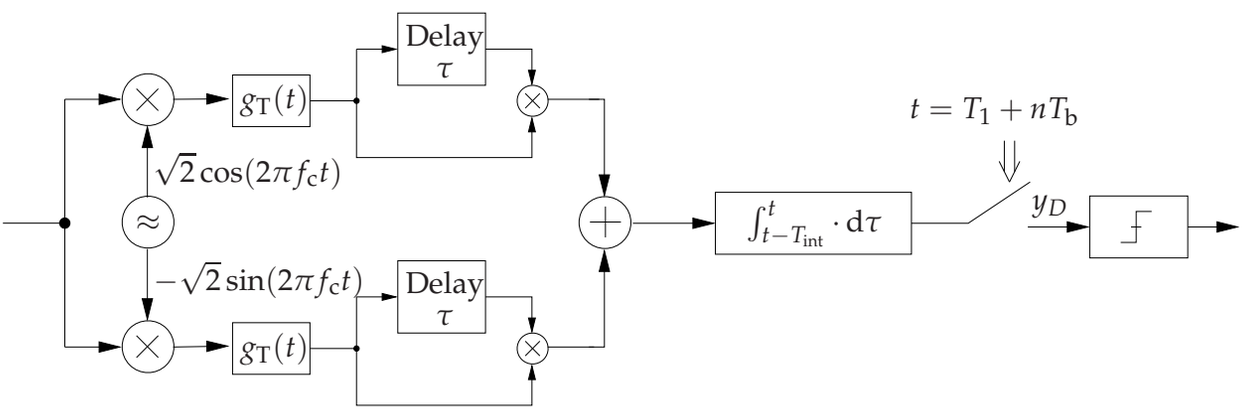

Figure 4. Differential detection for DPSK ($\tau = T_b$) or transmitted-reference PSK ($\tau < T_b$).

In the following, we consider binary pulse-position modulation (2-PPM) and differential phase-shift keying (DPSK) as straightforward modulation schemes to be combined with either envelope detection or with differential detection.

If E_b denotes the mean energy per bit, a 2-PPM signal (single carrier with fixed carrier frequency) given in the complex baseband can be written as

$$s(t) = \sqrt{E_b} \sum_{n=-\infty}^{\infty} (1 - b_n)\psi_1(t - nT_b) + b_n \psi_1(t - nT_b - T_b/2), \tag{1}$$

where $\psi_1(t)$ needs to be orthogonal to $\psi_1(t - T_b/2)$. T_b is the bit interval, which is split into two subintervals each of length $T_b/2$. Depending on the binary information b_n, $b_n \in \{0, 1\}$, to be transmitted, the waveform $\sqrt{E_b}\psi_1(t)$ is generated either at the time nT_b or $T_b/2$ seconds later. For single carrier transmission with a fixed carrier frequency, the unit energy basis function $\psi_1(t)$ needs to exhibit a bandwidth of at least 500 MHz, i.e., it is a spread spectrum waveform. For example, according to the IEEE 802.15.4a UWB PHY, $\psi_1(t)$ consists of a single

pulse with a duration of 2 ns (or less) or a burst of up to 128 such pulses with a scrambled polarity.

A (single carrier) DPSK signal given in the complex baseband can be written as

$$s(t) = \sqrt{E_\mathrm{b}} \sum_{n=-\infty}^{\infty} (2\tilde{b}_n - 1)\psi_1(t - nT_\mathrm{b}), \tag{2}$$

where $\tilde{b}_n = b_n \oplus \tilde{b}_{n-1}$, $\tilde{b}_n \in \{0, 1\}$, denotes differentially encoded bits.

2.1. Performance estimation for single-window combining

By increasing the transmission bandwidth B, more and more multipath arrivals are resolvable at the receiver. For example, with $B = 500$ MHz and an assumed excess delay of 50 ns, about 25 individual paths are resolvable in the time domain. In contrast to a channel matched filter (or its RAKE receiver equivalent), which combines all these arrivals coherently and with an appropriate weighting, the integrate and dump filter shown in Fig. 3 and Fig. 4 clearly allows only a non-coherent combining. This suboptimal combining leads to a performance loss, which increases with the product $B \cdot T_\mathrm{int}$, where it is assumed that the whole signal energy is contained within the integration interval T_int. If it is further assumed that $B \cdot T_\mathrm{int}$ is an integer $N \geq 1$, the BER p_b for 2-PPM (energy detection) can be estimated as [5]

$$\begin{aligned} p_\mathrm{b} &= \frac{1}{2^N} \exp\left(-\frac{E_\mathrm{b}}{2N_0}\right) \sum_{i=0}^{N-1} \frac{1}{2^i} \mathcal{L}_i^{N-1}\left(-\frac{E_\mathrm{b}}{2N_0}\right) \\ &\approx \frac{1}{2}\mathrm{erfc}\left(\frac{E_\mathrm{b}/N_0}{2\sqrt{E_\mathrm{b}/N_0 + N}}\right), \end{aligned} \tag{3}$$

where $\mathcal{L}_i^{N-1}$ is a generalized Laguerre polynomial. The second expression corresponds to a Gaussian approximation which can be used for $N > 15$. Eqn. (3) is only valid if the integration interval T_int contains the whole bit energy E_b, and if no ISI occurs, which is the case if the channel excess delay is small compared to T_b. The compact solution (3) has its origin in the fact that the samples y_0 and y_1 (see Fig. 3) are χ^2-distributed with $2N$ degrees of freedom [10].

For DPSK and differential detection, the statistical description is very similar. Thus, it is only required to substitute N_0 by $N_0/2$ in (3), i.e., the E_b/N_0-performance differs by exactly 3 dB in favor of DPSK.

Fig. 5 shows the penalty with respect to the required E_b/N_0, if we switch from — rather hypothetical — coherent channel matched filter detection to non-coherent detection with equal gain single-window combining (SinW-C). A value of 1.2 dB at $N = 1$ just corresponds to the E_b/N_0-penalty in AWGN ($p_\mathrm{b} = 10^{-3}$).

The results must be interpreted very carefully, since it is assumed that the whole bit energy is concentrated within the interval T_int. In reality, this is surely not the case and an appropriate T_int must be found. If T_int is increased, more and more noise is integrated which leads to the loss shown in Fig. 5, but more signal energy may be collected as well.

From the energy efficiency point of view, any non-coherent combining should take place with respect to the multipath energy only. If chirp or direct sequence spread spectrum (DSSS) signals are used, where the signal energy is spread over time even at the transmitter, it is

preferable to equip the receiver with a matched filter $g_T(t)$ which focuses the energy of the chirp or DSSS-waveform before the non-coherent processing takes place, as it was assumed in Fig. 3 and Fig. 4.

Fig. 6 shows the E_b/N_0-performance of 2-PPM in the case of a non-LOS indoor channel, where E_b is interpreted as the bit energy available at the receiver's antenna output. For the results shown, we have used measured UWB channels (5m×5m×2.6m office) including the antennas. The measurements were carried out by the IMST GmbH [6, 7]. B_6 is chosen to be 500 MHz.

The results show that the BER strongly depends on T_{int}, whereas the position of the integration window is always chosen optimally. For the reference indoor channel considered here [10], the optimal value of T_{int} is about 20 ns. At $T_{int} = 20$ ns, SinW-C loses additionally 1.5 dB compared to an optimal non-coherent detector, cf. Section 2.3.

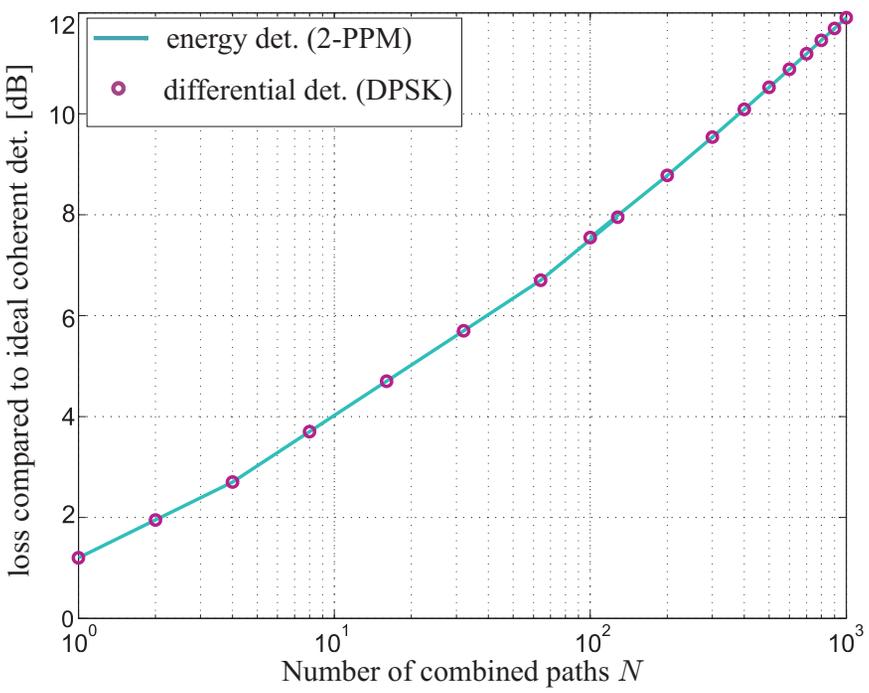

Figure 5. Power penalty due to non-coherent combining as a function of the time bandwidth product N ($p_b = 10^{-3}$). Coherent matched filter detection acts as the reference.

2.2. Weighted sub-window combining

In the case of SinW-C, at least two parameters need to be adjusted, the window size T_{int} and its position T_1 (synchronization). Since the BER over T_{int} performance of SinW-C may also exhibit several local minima, the practical determination of appropriate T_{int} and T_1 values may be more difficult than it seems. These problems are reduced, if weighted sub-window combining (WSubW-C) is used, where the whole integration window is divided into a number of N_{sub} sub-windows of size T_{sub}. From the E_b/N_0 performance point of view, it is preferable to choose the N_{sub} weighting coefficients according to the sub-window energies. In [10] we have shown that WSubW-C with $T_{sub} = 4$ ns (which corresponds to a sampling rate of 250 MHz) outperforms SinW-C (with optimum synchronization) by about 0.5 dB, if indoor channels are considered.

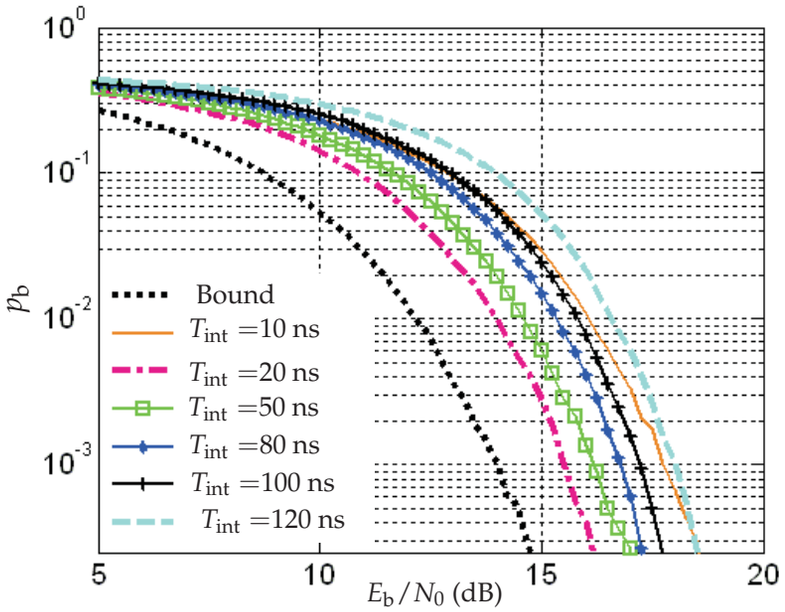

Figure 6. BER performance of non-coherent 2-PPM detection for SinW-C and a 6 dB signal bandwidth of 500 MHz. A measured indoor non-LOS channel is used to obtain the results.

2.3. Performance limit

If the sampling rate of the WSubW-C is equal to the signal bandwidth B, i.e., $T_{sub} = 1/B$, each resolvable multipath component[2] can be weighted according to its energy. In [10] we have shown that this approach ensures the benchmark performance, if non-coherent combining is used. The advantage compared to perfectly synchronized SinW-C is about 1.5 - 2 dB for indoor channels, cf. Fig. 6 (black, dotted curve).

3. Analog receiver implementations

3.1. Feasibility of analog differential detection

ISI will degrade the BER performance of DPSK systems, if the symbol interval is considerably smaller than the channel excess delay. However, it is crucial to realize delays on the order of 50 ns or more in the analog domain, if the ultra-wideband nature of the signals is taken into account. Fig. 7 shows the normalized group delay of a Bessel-Thomson all-pass filter with a maximum flat group delay $t_g(f)$. If a 5 % group delay error is chosen to define the cut-off frequency, it is clear that a 5th order filter can provide a usable frequency range of $\approx 1/t_g(0)$, i.e., for a desired cut-off frequency of $f_g = B_6/2 = 250$ MHz, the delay is only 4 ns. Even a huge and completely unrealistic filter order of 20 could only provide a delay of $5.6 \cdot 4 = 22$ ns, if $f_g = 250$ MHz. It should be noted that two of these analog delay lines have to be implemented, if a quadrature down-conversion stage as shown in Fig. 4 is used.

A basic motivation of impulse radio based on transmitted reference (TR) signaling is that shorter delays can be used. This is possible, since the autocorrelation does not take place with the previous modulated symbol but rather with an additional reference pulse. Our results show that the performance of TR-signaling varies extremely from channel realization

[2] At a total transmission bandwidth B, multipath components can be resolved down to $1/B$ in the time domain.

to channel realization, since the autocorrelation process is disturbed by intra-symbol interference. Additionally, if a reference pulse is periodically inserted prior to each modulated pulse, a 3 dB loss occurs. Delay hopping techniques or reference symbol averaging may reduce this 3 dB loss, but require even more (and longer) delay lines.

It is more than unlikely that analog implementations of differential receivers will have a chance to be applied in low cost products. For the multi-user case with analog multipath combining (next section), we have therefore focused on energy detection combined with time-hopping (TH) impulse radio.

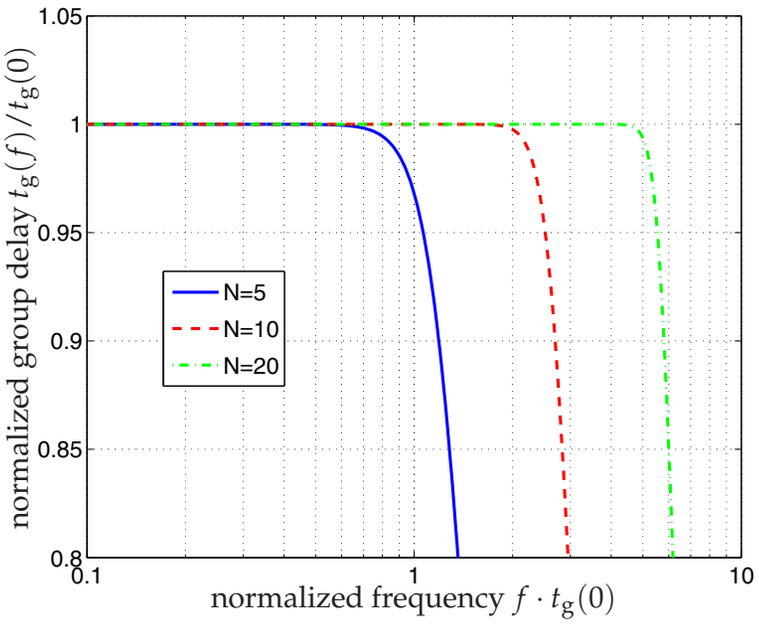

Figure 7. Normalized group delay of a Bessel-Thomson all-pass filter of order N.

3.2. Multiple access for analog multipath combining

As mentioned above, the transmitted pulse $\psi_1(t)$ may be also a chirp or direct-sequence spread spectrum waveform. To realize the filter $g_T(t)$ in the analog domain, SAW-filters (SAW: surface acoustic wave) could be a solution, but only if $\psi_1(t)$ is a fixed, user independent waveform. Therefore, as long as the non-coherent signal processing (or a part of it) takes place in the analog domain, we assume a user independent $\psi_1(t)$.

To still enable multiple access (MA) communications, we assume that each symbol to be transmitted is represented by several short pulses which are generated at distinct times according to a user specific TH-code. The decoding will be carried out digitally, i.e., after the non-coherent signal processing took place, cf. Fig. 8.

Compared to direct sequence MA codes which contain a large number of (non-zero) chips, the sparseness of TH codes facilitates the receiver processing, reduces the complexity and keeps the additional loss due to the non-coherent combining of the code elements within limits. A TH code is determined by two parameters: the number of pulse repetitions N_s, which is equivalent to the code weight, and the number of hopping positions[3] N_h. In [12], we have presented a semi-analytical method to assess the multiple access performance. It

[3] One symbol interval can be divided into an integer number N_s of equally spaced intervals (named frames), where each frame contains one pulse. Within each frame, N_h positions are possible.

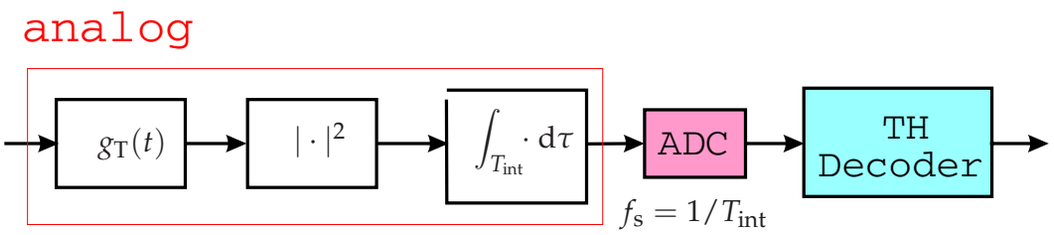

Figure 8. Block diagram of a TH code division multiple access receiver with analog multipath combining. Differential detection is not considered since analog wide band delays are difficult to realize.

is based on the statistics of the total code collisions (or "hits", determined by N_s and N_h) as well as the first- and second-order moments of the multipath channel's energy within the integration window. For non-coherent TH-PPM systems, the proposed method provides a more accurate and comprehensive evaluation of the multiple access performance than the existing code correlation function based analysis.

In [12], we have investigated various MA codes to be applied for a non-coherent TH-PPM system. It can be concluded that for a moderate number of users, optical orthogonal codes (truncated Costas codes, prime codes) with low code weights ensure a good multiple access performance while adding only a very small additional non-coherent combining loss.

4. Digital receiver implementations

Digital receiver implementations according to Fig. 9 have several advantages. First of all, they offer a superior interference rejection capability [11, 16], since user specific filtering can take place prior to the non-coherent signal processing. This restricts the non-coherent combining loss to the multipath arrivals (which exhibit stochastic path weights), whereas that part of the signal energy, which is already spread by a user-specific code at the transmitter, is coherently summed up. Furthermore, digital receiver implementations enable advanced modulations such as Walsh-modulation [15, 17] or advanced NBI-suppression strategies based on soft-limiting [13].

The block diagram of a receiver with a "digital code matched filter" (DCMF) is shown in Fig. 9. The ADC operates with a sampling rate, which is not smaller than the UWB signal bandwidth, where the ADC resolution has been chosen between 1 and 4 bits. Regarding the following results, we have always assumed TH impulse radio transmission.

Fig. 10 shows the E_b/N_0 improvement of a DCMF-based receiver as a function of N_s, where N_s depicts the number of non-zero elements of the user-specific code. As the DCMF combines the corresponding pulses coherently, the benefit compared to an analog receiver increases with N_s.

4.1. Applicability of low-resolution ADCs (single user case)

In [14] we have shown that in the 2-PPM case and under certain conditions, low-resolution ADCs can almost achieve the full resolution E_b/N_0-performance. One important condition is the number of pulse repetitions N_s within one modulated symbol, which should not be too small. For the one bit ADC case, $N_s = 8$ and $N_s = 20$ just correspond to quantization penalties of 2 dB and 1.5 dB, respectively, cf. Fig. 11(a). If the resolution is increased from 1 bit to 2 or 4 bits, the penalty may decrease, but only if the input level of the ADC is well controlled by an additional gain-control circuit. In [14] we have also proven that a 1 bit ADC with its inherent clipping characteristic offers a superior interference rejection capability.

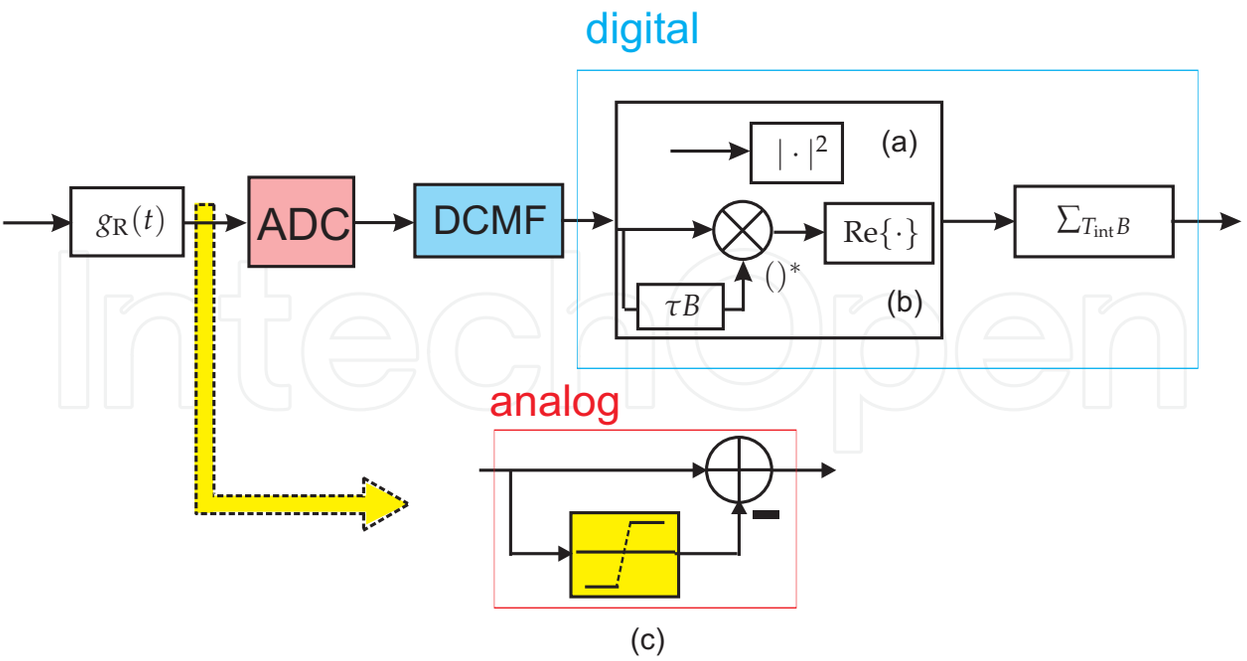

Figure 9. Block diagram of the DCMF-based non-coherent receiver shown in the complex baseband for (a) energy detection and (b) differential detection. (c) A NBI suppression scheme using a soft-limiter.

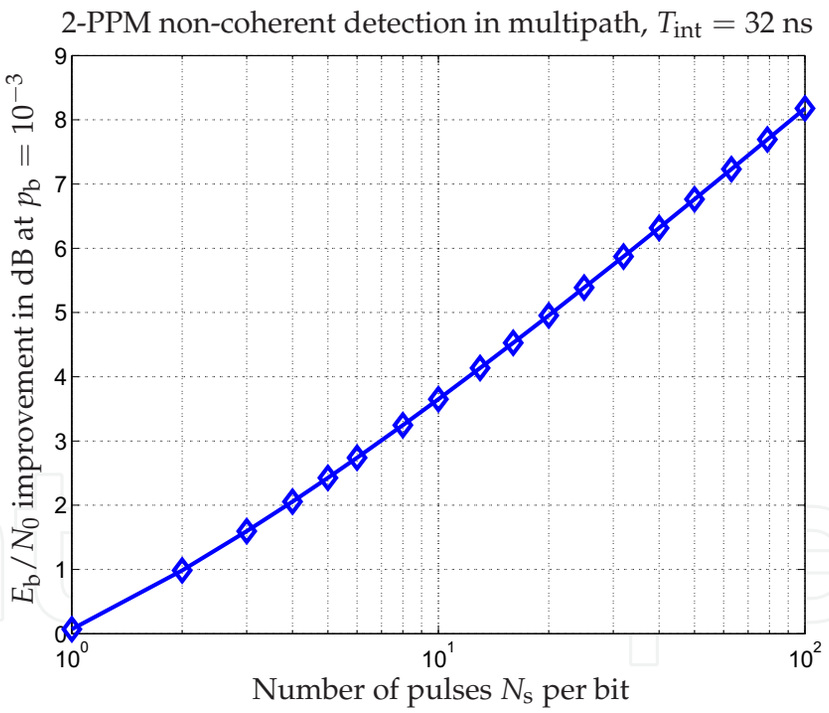

Figure 10. E_b/N_0 performance improvement of a fully digital 2-PPM non-coherent receiver compared to its analog counterpart for the multipath single-user case. The integration window extents over $T_{\mathrm{int}} = 32$ ns. A full-resolution ADC is assumed.

We have also investigated the applicability of Sigma-Delta ADCs, especially if M-ary Walsh modulation is used, cf. Section 4.4. The results show that the full resolution performance can be obtained for an oversampling rate of 4. Since the power consumption of an ADC depends linearly on the sampling rate, but exponentially on the resolution [8], Sigma-Delta ADCs can thus be considered as attractive candidates.

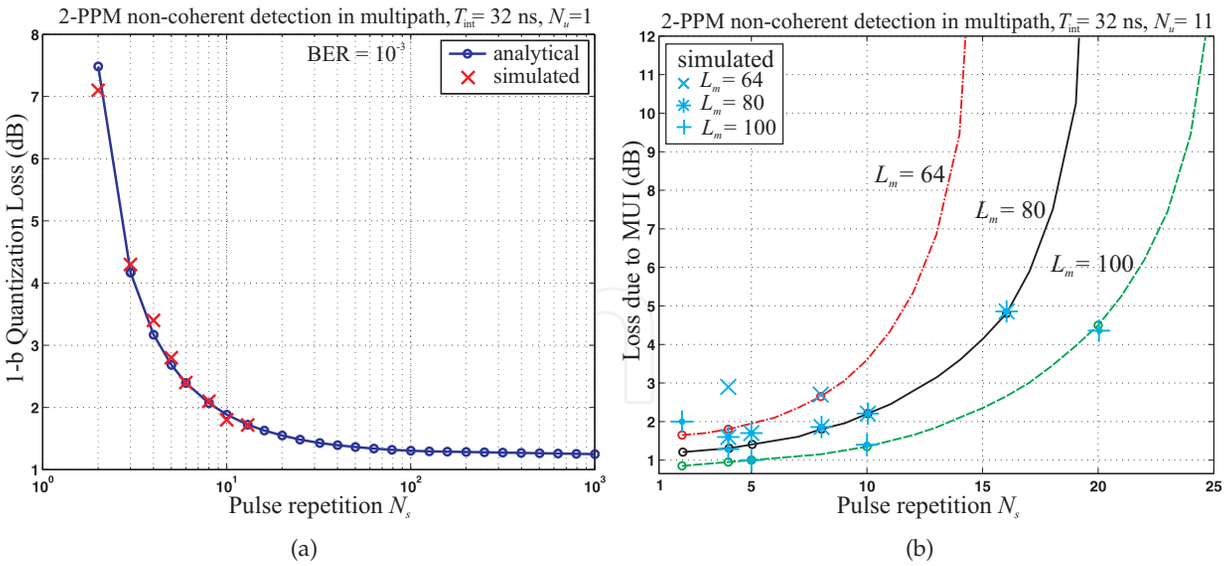

Figure 11. Power penalty due to 1-bit quantization (a) and multi-user interference (b), where random-codes are assumed. BER is 10^{-3}.

4.2. Multiple access codes for time hopping PPM

Fig. 11(b) shows the power penalty due to MUI for a network with 11 users, where perfect transmit power control and a full resolution ADC was assumed. Random codes were applied. For a given processing gain $N_s \cdot N_h$, the penalty depends strongly on the ratio of the parameters N_s (number of non-zero pulses) and N_h (number of hopping positions). Since N_s determines the ADC quantization induced penalty, too, we conclude that N_s on the order of 8 leads to a good trade-off between the quantization loss and the MUI penalty. In [14] we have shown that this rule does not only apply to random codes but also to optical orthogonal codes as suggested for analog receiver implementations.

4.3. Performance of simultaneously operating piconets

A test geometry of simultaneously operating piconets (SOP) is shown in Fig. 12, where a single co-channel interference is considered. The reference distance d_{ref} (desired piconet 1) is chosen such that the power at the receiver is 6 dB above the receiver sensitivity threshold. The interfering transmitter (uncoordinated piconet 2) operates at the same power as the transmitter of piconet 1, but at a distance d_{int} to the reference receiver. We have considered the IEEE 802.15.4a channel model 3 (indoor LOS) and the channel model 4 (indoor non-LOS) [9], where random TH codes with $N_s = 10$ and $N_h = 8$ are applied altogether with forward error correction (Reed Solomon code with a rate of 0.87). The results shown in Table 1 prove clearly that digital receiver implementations outperform analog ones. Furthermore, 1-bit ADCs are desirable.

Channels	Analog	DCMF (full)	DCMF (1 bit)
CM3	1.53	0.64	0.32
CM4	1.05	0.71	0.45

Table 1. d_{int}/d_{ref} at 1% packet error ratio for SOP tests

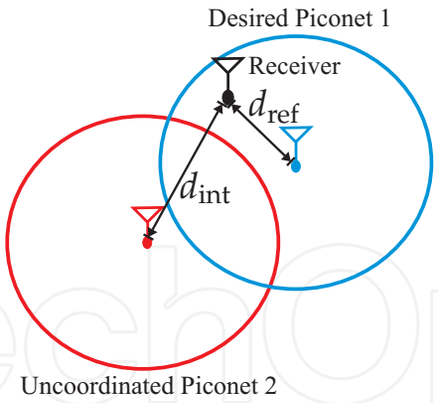

Figure 12. The SOP test geometry with a single co-channel interference

4.4. Power efficient Walsh-modulation

In [17], we have proposed two advanced (low data rate) transmission schemes based on M-ary Walsh-modulation, namely repeated Walsh (R-Walsh) and spread Walsh (S-Walsh). For both schemes, the fast Walsh Hadamard transformation can be used to efficiently implement the demodulator. Whereas the more implementation friendly R-Walsh transmission is favorable for data rates of up to 180 kbps ($M = 8$ or $M = 16$), S-Walsh transmission with $M \geq 32$ is an option for higher data rates.

In [15], we have compared R-Walsh transmission with M-PPM. It has been shown that R-Walsh works well with a 1-bit quantization. Fig. 13 shows that in the case of Walsh modulation, the quantization loss (compared to the full resolution case) is only about 1.5 dB — independently of M and N_s. However, if a strong near-far effect is present, M-PPM outperforms R-Walsh with respect to the MA-performance.

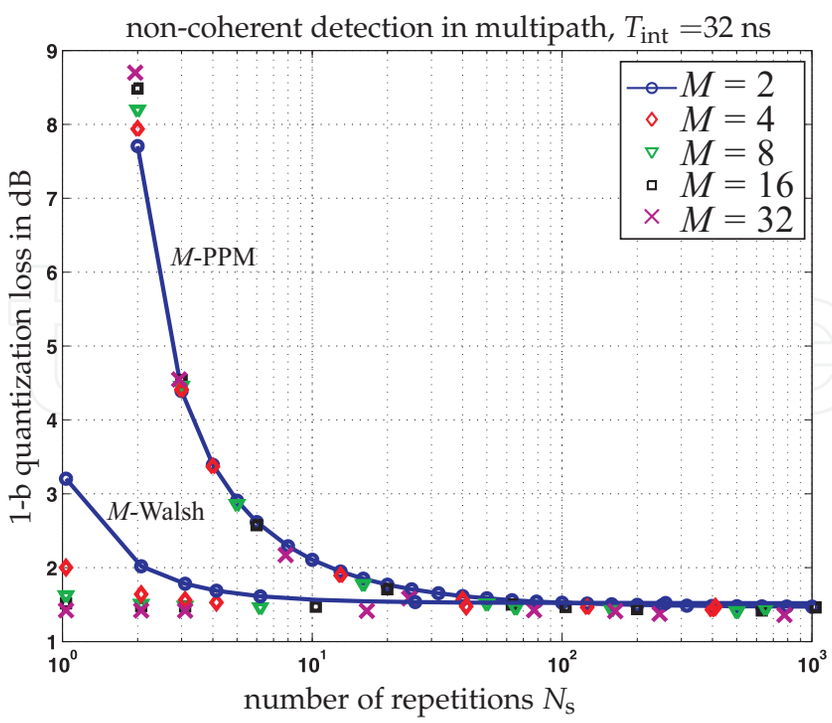

Figure 13. Quantization loss due to a one-bit ADC versus the number of repetitions N_s at $p_b = 10^{-3}$ for M-Walsh and M-PPM in multipath channels (analytical estimation).

4.5. Advanced narrowband interference suppression schemes

In [13] we have presented a new NBI-mitigation technique, which is shown in Fig. 9c). It is based on a soft limiter, where the soft limiter itself was originally proposed to suppress impulse interference [2]. The thresholds of the soft limiters are adjusted according to NBI power.

We have shown that the proposed receiver can effectively mitigate the NBI, if the threshold factor and the input level of the subsequent ADC are chosen appropriately. Furthermore, the performance improves if the ADC resolution is increased. In the presence of the OFDM interference, the proposed scheme could also be used, but it is required to adjust the threshold dynamically. It should be noted that the performance also depends on the frequency of the interference, since the DCMF has a frequency dependent transfer function.

5. Conclusions

We have derived concepts for energy efficient impulse radio UWB systems with a low transceiver complexity. These concepts are especially suitable for wireless sensor networks operating at low data rates. The E_b/N_0-performance of non-coherently detected 2-PPM and DPSK is very similar. It differs by 3 dB in favour of DPSK. However, if the multipath combining should take place in the analog domain, i.e., by means a simple integrate and dump filter, the difficulty to realize analog broadband delays makes it almost impossible to use differential detection and thus DPSK. On the contrary, digital receiver implementations enable advanced modulation schemes and offer superior interference rejection capabilities. With low-resolution ADCs, only a small quantization loss is observed. Compared to the full-resolution case, a one-bit receiver shows a higher MUI suppressing capability. Sigma-Delta ADCs can be considered as attractive candidates for the analog to digital conversion. Our results show that the full resolution performance can be obtained for an oversampling rate of 4.

Author details

Nuan Song, Mike Wolf and Martin Haardt
Ilmenau University of Technology, Germany

6. References

[1] 05-58, F. [2005]. Petition for Waiver of the Part 15 UWB Regulations Filed by the Multi-band OFDM Alliance Special Interest Group, ET Docket 04-352.
[2] Beaulieu, N. C. & Hu, B. [2008]. Soft-Limiting Receiver Structures for Time-Hopping UWB in Multiple Access Interference, *IEEE Transactions on Vehicular Technology* 57.
[3] Commission, F. C. [2002]. First Report and Order: Revision of Part 15 of the Commission's Rules Regarding Ultra-Wideband Transmission Systems, ET Docker 98-153.
[4] ECC [2007]. ECC Decision of 24 March 2006 amended 6 July 2007 at Constanta on the harmonised conditions for devices using Ultra-Wideband (UWB) technology in bands below 10.6 GHz, amended ECC/DEC/(06)04.

[5] Hao, M. & Wicker, S. [1995]. Performance evaluation of FSK and CPFSK optical communication systems: a stable and accurate method, *Journal of lightwave technology* (13): 1613–1623.

[6] Kunisch, J. & Pamp, J. [2002]. Measurement Results and Modeling Aspects for the UWB Radio Channel, *IEEE Conference on Ultra Wide-Band Systems and Technologies* .

[7] Kunisch, J. & Pamp, J. [n.d.]. *IMST-UWBW: 1-11 GHz UWB Indoor Radio Channel Measurement Data*, IMST GmbH. available at http://www.imst.com/imst/en/research/radio-networks/funk_wel_dow.php.

[8] Le, B., Rondeau, T. W., Reed, J. H. & Bostian, C. W. [2005]. Analog-to-digital converters, *IEEE Signal Processing Magazine* 22(6): 69–77.

[9] Molisch, A. F. et al. [2005]. IEEE 802.15.4a channel model - final report, *Tech. Rep. Document IEEE 802.15-04-0662- 02-004a*.

[10] Song, N., Wolf, M. & Haardt, M. [2007]. Low-complexity and Energy Efficient Non-coherent Receivers for UWB Communications, *Proc. 18-th Annual IEEE International Symposium on Personal Indoor and Mobile Radio Communications (PIMRC07)*, Greece.

[11] Song, N., Wolf, M. & Haardt, M. [2009a]. A Digital Code Matched Filter-based Non-Coherent Receiver for Low Data Rate TH-PPM-UWB Systems in the Presence of MUI, *IEEE International Conference on Ultra Wideband (ICUWB 2009)*, Vancouver, Canada.

[12] Song, N., Wolf, M. & Haardt, M. [2009c]. Performance of PPM-Based Non-Coherent Impulse Radio UWB Systems using Sparse Codes in the Presence of Multi-User Interference, *Proc. of IEEE Wireless Communications and Networking Conference (WCNC 2009)*, Budapest, Hungary.

[13] Song, N., Wolf, M. & Haardt, M. [2010a]. A Digital Non-Coherent Ultra-Wideband Receiver using a Soft-Limiter for Narrowband Interference Suppression, *Proc. 7-th International Symposium on Wireless Communications Systems (ISWCS 2010)*, York, United Kingdom.

[14] Song, N., Wolf, M. & Haardt, M. [2010b]. A *b*-bit Non-Coherent Receiver based on a Digital Code Matched Filter for Low Data Rate TH-PPM-UWB Systems in the Presence of MUI, *Proc. of IEEE International Conference on Communications (ICC 2010)*, Cape Town, South Africa.

[15] Song, N., Wolf, M. & Haardt, M. [2010d]. Time-Hopping M-Walsh UWB Transmission Scheme for a One-Bit Non-Coherent Receiver, *Proc. 7-th International Symposium on Wireless Communications Systems (ISWCS 2010)*, York, United Kingdom.

[16] Song, N., Wolf, M. & Haardt, M. [Feb., 2009b]. Non-coherent Receivers for Energy Efficient UWB Transmission, *UKoLoS Annual Colloquium*, Erlangen, Germany.

[17] Song, N., Wolf, M. & Haardt, M. [Mar., 2010c]. Digital non-coherent UWB receiver based on TH-Walsh transmission schemes, *UKoLoS Annual Colloquium*, Günzburg , Germany.

[18] TG4a, I. . [2007]. Part 15.4: Wireless Medium Access Control (MAC) and Physical Layer (PHY) Specifications for Low-Rate Wireless Personal Area Networks (WPANs), *IEEE Standard for Information Technology* .

[19] Wolf, M., Song, N. & Haardt, M. [2009]. Non-Coherent UWB Communications, *FREQUENZ Journal of RF-Engineering and Telecommunications* . special issue on Ultra-Wideband Radio Technologies for Communications, Localisation and Sensor applications.